Pharmaceutical Research, Vol. 23, No. 4, April 2006 (© 2006)
DOI: 10.1007/s11095-006-9609-x

Research Paper

Effective Targeting of Liposomes to Liver and Hepatocytes *In Vivo* by Incorporation of a *Plasmodium* Amino Acid Sequence

Kenneth J. Longmuir,[1,4,5] Richard T. Robertson,[2,4] Sherry M. Haynes,[1] Janie L. Baratta,[2] and Alan J. Waring[3]

Received October 10, 2005; accepted November 28, 2005

Purpose. Several species of the protozoan *Plasmodium* effectively target mammalian liver during the initial phase of host invasion. The purpose of this study was to demonstrate that a *Plasmodium* targeting amino acid sequence can be engineered into therapeutic nanoparticle delivery systems.
Methods. A 19-amino peptide from the circumsporozoite protein of *Plasmodium berghei* was prepared containing the conserved region I as well as a consensus heparan sulfate proteoglycan binding sequence. This peptide was attached to the distal end of a lipid–polyethylene glycol bioconjugate. The bioconjugate was incorporated into phosphatidylcholine liposomes containing fluorescently labeled lipids to follow blood clearance and organ distribution *in vivo*.
Results. When administered intravenously into mice, the peptide-containing liposomes were rapidly cleared from the circulation and were recovered almost entirely in the liver. Fluorescence and electron microscopy demonstrated that the liposomes were accumulated both by nonparenchymal cells and hepatocytes, with the majority of the liposomal material associated with hepatocytes. Accumulation of liposomes in the liver was several hundredfold higher compared to heart, lung, and kidney, and more than 10-fold higher compared to spleen. In liver slice experiments, liposome binding was specific to sites sensitive to heparinase.
Conclusions. Incorporation of amino acid sequences that recognize glycosaminoglycans is an effective strategy for the development of targeted drug delivery systems.

KEY WORDS: drug delivery; hepatocytes; liposomes; liver; targeting.

INTRODUCTION

Targeting of therapeutic nanoparticles to specific organs, tissues, or sites of tumors *in vivo* is an important goal of current efforts to develop drug delivery systems. The liver is particularly well suited for nanoparticle targeting and uptake, as the open and relatively large fenestrations of the endothelial lining of the sinusoids allow for the greater possibility of particle extravasation, compared to the capillary beds of most other organ systems (1,2).

In nature, a remarkably effective liver-targeting strategy is exhibited by the protozoans *Plasmodium falciparum*, *P. vivax*, *P. ovale*, and *P. malariae*, which infect humans, and two related species that infect rodents, *P. berghei* and *P. yoelii* (3–5). When introduced into the circulation, the sporozoite stage of the organism is cleared by the liver within minutes (6), and infection with as few as ten sporozoites can subsequently lead to malaria (7). The organ specificity is attributed to two major surface proteins on the sporozoite, circumsporozoite protein (CSP) and thrombospondin-related anonymous protein (4,5). The CSP contains two conserved amino acid sequences (termed regions I and II) that are found in the various species that infect mammalian hosts (8). Recently, a peptide containing the conserved region I amino acids (KLKQP) plus the basic amino acid domain upstream from region I has been shown to bind strongly to affinity columns of heparin and heparan sulfate (9). It is proposed that this 19-amino-acid sequence of the CSP of *P. falciparum* is at least partially responsible for *Plasmodium* targeting *in vivo* by binding to the highly sulfated heparan sulfate proteoglycans (HSPGs) found in liver (9,10). These HSPGs are located primarily on the basolateral side of the hepatocytes and within the space of Disse (11,12).

Numerous cellular and physiological functions are regulated by interactions between ligands and HSPGs (13,14). In addition, adherence to proteoglycans is exploited by a variety of microorganisms as an initial step of host invasion, often in a highly cell-specific or organ-specific fashion (15). In contrast, incorporation of proteoglycan recognition into targeted drug and gene delivery systems has been quite limited (16–18). For this investigation, it was our hypothesis that a peptide containing an amino acid sequence from an HSPG-

[1] Department of Physiology and Biophysics, School of Medicine, University of California, Irvine, California 92697, USA.
[2] Department of Anatomy and Neurobiology, School of Medicine, University of California, Irvine, California 92697, USA.
[3] Departments of Medicine and Pediatrics, School of Medicine, University of California, Los Angeles, California 90095, USA.
[4] K. J. Longmuir and R. T. Robertson were the primary investigators for this study.
[5] To whom correspondence should be addressed (e-mail: longmuir@uci.edu)

ABBREVIATIONS: ASGP-R, asialoglycoprotein receptor; CSP, circumsporozoite protein; HSPG, heparan sulfate proteoglycan.

binding region of plasmodium CSP could be engineered into liposome formulations that would selectively target the liver *in vivo*. Here we report that we have successfully developed liposome formulations containing a peptide with an amino acid sequence from the region I domain of the CSP of *P. berghei*. When administered systemically in mice, we found that peptide-containing liposomes were rapidly cleared from the blood and were targeted specifically to the liver, with the majority of the liposomal material associated with hepatocytes.

MATERIALS AND METHODS

Peptide Synthesis

The peptide acetyl-CKNEKKNKIERNNKLKQPP-amide consisted of an N-terminal acetylcysteine followed by amino acids 76–93 of the N-terminal region of the CSP of *P. berghei*, Anka strain (Swiss-PROT entry name, CSP_PLABA; primary accession no. P23093). This peptide was synthesized by Fmoc chemistry using a FastMoc™ protocol (19). Cleavage from the resin and purification were performed as described previously (20,21). Mass spectrometry was performed using alpha matrix [α-cyano-4-hydroxycinnamic acid (22)] in an ABI Voyager DE-STR MALDI-TOF instrument operating in reflectance mode, with positive polarity, delayed extraction, and an acquisition range of 1100 to 3000 Da. The mass spectrum exhibited a single molecular species with the correct mass + 1 of 2351 Da (100% carbon-12) followed by additional intensities at 2352–2355 corresponding to the expected binomial distribution of one, two, three, and four atoms of carbon-13.

Lipid Synthesis

1,2-Dierucoyl-*sn*-3-phosphatidylcholine (di22:1-PC) was obtained from Avanti Polar Lipids (Alabaster, AL, USA). 1,2-Dierucoyl-*sn*-3-phosphatidylethanolamine (di22:1-PE) was synthesized by base exchange of di22:1-PC with ethanolamine, catalyzed by *Streptomyces* sp. phospholipase D (Sigma, St. Louis, MO, USA) (23).

The synthesis of 1,2-dierucoyl-*sn*-3-aminopropane (di22:1-AP) was carried out in three steps. First, *sn*-3-aminopropanediol (Aldrich, Milwaukee, WI, USA) was converted to *sn*-3-(*t*-BOC)aminopropanediol by reacting with 2-(*tert*-butoxycarbonyloxyimino)-2-phenylacetonitrile (Boc-ON, Aldrich, Milwaukee, WI, USA) according to the protocols provided by the manufacturer. The product was acylated with erucic acid to form 1,2-dierucoyl-*sn*-3-(*t*-BOC)aminopropane by standard carbodiimide chemistry with dimethylaminopyridine catalyst (24), then purified by LH-20 Sephadex chromatography in a solvent system of reagent alcohol/water (95:5). The *t*-BOC group was then removed in dichloromethane/trifluoroacetic acid (90:10) to form 1,2-dierucoyl-*sn*-3-aminopropane, and the product purified by removal of volatile compounds by drying *in vacuo* for 24 h.

The $mPEG_{5000}$ conjugate of 22:1-PE was prepared by reacting 10 μmol di22:1-PE with 20 μmol of $mPEG_{5000}$ carboxylic acid *N*-hydroxysuccinimidyl ester (2M4M0H01, Nektar, Huntsville, AL, USA) and 100 μmol of triethylamine in dichloromethane. The product was purified by repeated precipitation in *t*-butyl methyl ether, followed by separation from excess free $mPEG_{5000}$ by column chromatography on G-75 Sephadex in distilled water. Thin-layer chromatography analysis (chloroform/methanol 16:3) of the column fractions indicated complete separation of the lipid–PEG conjugate from free PEG due to the propensity of lipid–PEG conjugates to form higher molecular weight micelles in water. The maleimide-PEG_{3400} conjugate of di22:1-AP was prepared in the same fashion, using maleimide-PEG_{3400} carboxylic acid *N*-hydroxysuccinimidyl ester (Nektar 2E4M0F02). The C6-maleimide conjugate of di22:1-AP was prepared by reacting 10 μmol di22:1-AP with 20 μmol of the heterobifunctional cross-linker EMCS (Pierce Chemical Company, Rockford, IL, USA) and 100 μmol triethylamine. This product was purified by chromatography on LH-20 Sephadex in a solvent of distilled reagent alcohol.

Fluorescent lipids were prepared by reacting, in a typical preparation, 2 μmol di22:1-AP with 3 μmol Bodipy-FL STP ester or 3 μmol Bodipy-TR-X SE ester (Molecular Probes, Eugene, OR, USA) with 10 μmol triethylamine in 200 μL dimethylformamide. The fluorescent lipid product was purified by LH-20 Sephadex chromatography in reagent alcohol/water (95:5). Concentrations were determined by absorbance (504 nm for Bodipy-FL, ε = 68,000 M^{-1} cm^{-1}; 585 nm for Bodipy-TR-X, ε = 80,000 M^{-1} cm^{-1}).

For the preparation of di22:1-AP–PEG_{3400}–succinyl peptide conjugate, 4 μmol of the peptide in dimethylformamide was titrated with aliquots of di22:1-AP–maleimide-PEG_{3400} (also dissolved in dimethylformamide) until DTNB analysis showed less than 2% of the initial concentration of free cysteine. The di22:1-AP–C6-succinyl peptide was prepared in the same fashion from di22:1-AP–C6-maleimide.

1,2-Dipalmitoyl-*sn*-3-phosphatidylethanolamine labeled with 1.4-nm gold particles was obtained from Nanoprobes, Inc. (Yaphank, NY, USA).

Preparation of Liposomes

Aliquots of lipid, fluorescent lipid, lipid–PEG conjugate, and lipid–PEG–peptide conjugate were mixed, the solvents evaporated (N_2 gas), and then dried *in vacuo* at < 100 μbar pressure for > 1 h at room temperature. For biophysical studies, the lipid residues were suspended in 10 mM HEPES (pH 7.4) with 5% glucose (HEPES–glucose). For *in vivo* studies, the lipid residues were suspended in 5% glucose only. The suspension was treated with two freeze–thaw cycles, and then extruded 10× through a double stack of 80-nm Nuclepore filters (Whatman, Clifton, NJ, USA). The resulting liposomes were filter-sterilized through 0.22-μm filters before use. For *in vivo* studies, liposomes were concentrated by centrifugation at 4000 × *g* in sterile Amicon Ultrafree-MC centrifugal filter devices with Biomax 100,000 MWCO filters (Millipore, Bedford, MA, USA) and adjusted to a final concentration of 1 μmol liposomal lipid per 50 μL.

For analysis of contents leakage, liposomes were formed as above in the presence of 50 mM calcein. Free calcein dye was removed by column chromatography with G-100 Sephadex (20-mL bed volume).

Biophysical Measurements

For measurement of serum-induced aggregation, liposomes, 0.3 μmol in 0.3 mL of HEPES–glucose, were mixed

with 0.7 mL fetal calf serum, then incubated at 37°C. Turbidity was evaluated by absorbance at 500 nm over a 4-h period. Zero absorbance was set with HEPES–glucose alone. Control samples consisted of 0.7 mL serum plus 0.3 mL HEPES–glucose without liposomes.

Z-average size, polydispersity index, and zeta potential were measured using a Malvern Nano ZS instrument with Malvern disposable zeta cells (Malvern USA, Southborough, MA, USA). Solutions were typically 0.3 to 0.5 μmol liposomes in 1 mL HEPES–glucose.

In Vivo Studies

All *in vivo* protocols were reviewed and approved by the University of California, Irvine, Institutional Animal Care and Use Committee (IACUC) prior to conducting the experiments. BALB/c female mice, approximately 20–25 g, were injected via the tail vein with a mixture of 0.8 μmol of control liposomes (Table I) and 0.8 μmol peptide-containing liposomes (Table I) in 80 μL of 5% glucose. Blood samples were taken at 15-, 30-, 60-, and 90-min time points.

For collection of tissue, mice (n = 4) were deeply anesthetized with sodium pentobarbital (50 mg/kg i.p.), then perfused through the heart with 10 mL of 0.9% saline at a flow rate of 5 mL/min. Liver, lungs, spleen, kidneys, heart, and a small portion of adipose tissue were removed and placed in phosphate-buffered saline for subsequent lipid extraction and fluorescence measurements, as described next.

For light and electron microscopy, mice (n = 18) were euthanized by vascular perfusion at times of 15 min, 1 h, 1.5 h, and 4 h after the i.v. injections. Animals were perfused through the heart with saline followed by 25 mL 4% paraformaldehyde, using a perfusion pump at a rate of 5 mL/min. Samples of tissue were collected and cut into 2- to 3-mm-thick blocks. For light microscopy studies, tissue blocks were postfixed in 4% paraformaldehyde before being transferred to a 30% sucrose solution overnight at 4°C for cryoprotection. Tissue blocks were cut on a Reichert–Jung cryostat at a section thickness of 10–12 μm and sections were mounted directly onto subbed slides. Sections were inspected using a Nikon fluorescence microscope equipped with rhodamine and fluorescein filter sets. Images were captured using a Nikon DS 5M digital camera and imported into Adobe PhotoShop.

Liver tissue from three animals (euthanized 15 min, 1 h, and 4 h after i.v. injections of the labeled liposomes) was used for electron microscope studies. Following the saline perfusion and fixation, tissue was postfixed in 4% paraformaldehyde and 0.5% glutaraldehyde. Tissue blocks were cut on a Vibratome at 50 μm and sections were processed using a gold-enhancement kit (Goldenhance-EM Nanoprobes Inc., Yaphank, NY, USA) following the protocols described by the manufacturer. Sections were placed in 1% osmium tetroxide for 30 min, embedded in epoxy, cut at 800 nm, and stained with uranyl acetate and lead citrate to enhance contrast. These stained sections were inspected on a Phillips EM-10 electron microscope equipped with a Gatan digital camera.

Hepatocytes were easily identified in thin sections by their large size and polygonal structure. Endothelial and Kupffer cells forming the borders of sinusoids were identified using fine structural criteria (25–28). Kupffer cells contain more lysosomes than do endothelial cells, but do not express the fenestrations that are characteristic of endothelial cells. However, it was not always possible to identify conclusively the fragments of cells lining sinusoids that were visible in thin sections, and hence the quantitative analyses (see "Data Analysis") simply compared parenchymal (hepatocytes) and nonparenchymal (endothelial and Kupffer) cells.

Table I. Molecular components and formulations used in this investigation

Peptide
Acetyl-CKNEKKNKIERNNKLKQPP-amide (conserved region I sequence, KLKQP; consensus heparan sulfate binding sequence, EKKNKI)
Principal liposomal lipid
1,2-dierucoyl-*sn*-3-phosphatidylcholine (di22:1-PC)
Fluorescent lipids
1,2-dierucoyl-*sn*-3-(Bodipy-FL)-aminopropane (di22:1-AP-Bodipy-FL); λ_{ex} = 504 nm, λ_{em} = 515 nm
1,2-dierucoyl-*sn*-3-(Bodipy-TR-X)-aminopropane (di22:1-AP-Bodipy-TR-X); λ_{ex} = 585 nm, λ_{em} = 630 nm
Lipid–polyethylene glycol–peptide conjugate
1,2-dierucoyl-*sn*-3-(PEG_{3400}-succinyl-peptide)-aminopropane (di22:1-AP-PEG_{3400}–peptide)
Lipid–polyethylene glycol conjugate
1,2-dierucoyl-*sn*-3-(PEG_{5000})–phosphatidylethanolamine (di22:1-PE–PEG_{5000})
Formulation of peptide-containing liposomes for intravenous injection in mice[a]
82% di22:1-PC
10% di22:1-PE–PEG_{5000}
4% di22:1-AP–PEG_{3400}–peptide
4% di22:1-AP–Bodipy-TR-X
Size[b] by dynamic light scattering, 88.4 ± 0.1 nm; polydispersity index, 0.11 ± 0.01; zeta potential, +5.2 ± 0.2 mV
For electron microscopy: addition of 0.1% 1,2-dipalmitoyl-*sn*-3-phosphatidylethanolamine with 1.4-nm gold particle
Formulation of control liposomes for intravenous injection in mice[a]
86% di22:1-PC
10% di22:1-PE–PEG_{5000}
4% di22:1-AP–Bodipy-FL
Size[b] by dynamic light scattering, 106.8 ± 0.3 nm; polydispersity index, 0.07 ± 0.01; zeta potential: −6.5 ± 0.9 mV

[a] Percentages indicate mole fractions.
[b] Size, polydispersity index, and zeta potential measurements are mean ± SEM; n = 3.

Lipid Extraction and Fluorescence Analysis

The weights of the entire liver, lungs, spleen, kidneys, and heart were recorded, then portions of each tissue (0.05 to 0.2 g each) were weighed, homogenized in 1 mL phosphate-buffered saline with a Teflon-glass homogenizer, and the lipids extracted by modification of the method of Bligh and Dyer (29) as follows: The 1-mL homogenate solution was mixed with 3 mL methanol, 1 mL chloroform, and 100 μL acetic acid and allowed to stand at room temperature for 30 min. The solution was separated into two phases by the addition of 3 mL chloroform and 2 mL water, then centrifuged. The upper phase was removed, and the lower phase, containing the extracted lipids, was washed twice with 3 mL of methanol/water (1:1). The solvents of the lower phase were evaporated, and the lipid residue redissolved in 2.0 mL of chloroform/methanol (2:1). For comparison, a known quantity (typically 10 nmol) of the liposomes used for injection of the mice was extracted in exactly the same fashion.

Fluorescence spectra of the extracted tissue lipids were obtained with a Varian Eclipse fluorometer. Bodipy-FL was measured by excitation at 485 nm and scanning for emission from 500 to 600 nm. Bodipy-TR-X was measured by excitation at 585 nm and scanning for emission from 600 to 700 nm. For all samples, absorption spectra were obtained over the same wavelength regions (Varian Cary 50 spectrophotometer). Emission and absorption spectra were recorded digitally (0.5 nm step size) and imported into Excel spreadsheets. Fluorescence intensities were calculated by subtracting the spectrum of the solvent only, correcting the emission spectrum for inner filter effects using the method of Lakowicz (30), then integrating the spectrum over the 100-nm emission wavelength range (see Fig. 2B for representative emission spectra). Nanomoles of liposomes was calculated by comparison with the fluorescence emission spectrum of the extracted lipid from the aliquot of liposomes (of known quantity) used for injection.

Plasma fluorescence was obtained by centrifugation of the blood samples at 4000 × *g* for 5 min. Then, 3 μL of plasma was diluted to 1.0 mL with phosphate-buffered saline, and the Bodipy-FL and Bodipy-TR-X emission spectra recorded digitally as described above. The integrated fluorescence spectra were quantitatively compared to the spectra of a known quantity of injected liposomes, also diluted to 1.0 mL of phosphate-buffered saline.

Liposome Binding to Enzyme-Treated Liver Slices

Adult mice were perfused intravascularly with 0.9% saline (10 mL over 2 min) followed by 4% paraformaldehyde in 0.1 M sodium phosphate buffer (pH 7.4). Livers were removed and cut into 5-mm blocks, postfixed in 4% paraformaldehyde for 2 h, and then placed overnight in a 30% sucrose solution in 0.1 M sodium phosphate buffer. Liver tissue was cut on a cryostat at thickness of 10–12 μm and mounted directly onto slides.

Slices were rinsed in 0.1 M MOPS buffer (pH 7.0), and then exposed for 2 h at 37°C to solutions of heparinase in MOPS buffer, chondroitinase ABC in MOPS buffer, or control solutions of MOPS without enzyme added. After the enzyme (or control) treatment, the sections were rinsed three times in Tris-buffered saline before being exposed to control or peptide-containing liposomes (10 nmol/mL) for 1 h at room temperature. Sections were rinsed three times in Tris-buffered saline and then examined using a Nikon fluorescence microscope equipped with rhodamine or fluorescein filter sets. Sections were photographed with a Nikon digital camera, with the same exposure settings for enzyme and control treatments.

Data Analysis

Data for serum-induced aggregation of liposomes (Fig. 1A and B) were tested for significant differences using analysis of covariance. Data for resonance energy transfer (Fig. 1C) and calcein fluorescence (Fig. 1D) were tested for significant differences at their emission maxima using paired, two-tailed *t* tests. Data for liposome clearance from blood (Fig. 2A) were tested for significant differences by analysis of variance. Data for liposome uptake by various organs (Fig. 2C and D) were tested for significant differences between liver and other organs using paired, two-tailed *t* tests.

For quantitative analysis of gold particles in electron micrographs (Fig. 4), image files were imported into Adobe PhotoShop without modification and prints of images 15 × 15 cm were made with an Epson 980 Stylus printer. A graticule representing a 0.5-μm square with 0.05-μm subdivisions was overlaid over cytoplasmic regions of both parenchymal cells (hepatocyte) and nonparenchymal cells (endothelial + Kupffer) for counting gold particles. Numbers of particles were calculated per 0.25 μm^2 and averaged separately for parenchymal cells and nonparenchymal cells; the two average values were tested for a significant difference using a two-tailed, unpaired *t* test. In all, 69 regions from two to three ultrathin sections from each of the three animals were counted for parenchymal cells, and 42 regions were counted for nonparenchymal cells.

RESULTS

Table I summarizes the lipid and lipid–peptide components prepared for this investigation, their abbreviations, and the liposome formulations developed for *in vivo* administration. Most components contained 22-carbon acyl chains of erucic acid (22:1, *cis*-13). This monounsaturated fatty acid with a relatively long hydrocarbon chain length was chosen to obtain liposome formulations that were stable, by several criteria, in the presence of serum at 37°C. As shown in the following paragraphs, we obtained liposome formulations that did not aggregate in serum; the fluorescent lipids containing the 22:1 acyl chains did not partition into serum components, and the liposomes did not exhibit significant leakage of entrapped contents.

Prevention of Liposome Aggregation

It was important to demonstrate that liposome formulations developed for intravenous administration did not aggregate in serum, both for reasons of safety and to ensure their ability to cross the fenestrations of liver endothelium. However, we found that liposomes containing di22:1-PC plus di22:1-AP–peptide aggregated strongly upon mixing with

serum, and the solutions immediately became turbid. As shown by turbidity measurements (Fig. 1A) this aggregation occurred both when the peptide was linked to the di22:1-aminopropane through a short (six-carbon) acyl chain and when the peptide was attached to the distal end of a bioconjugate of di22:1-aminopropane–PEG_{3400}.

We found that liposome aggregation in the presence of serum could be eliminated by including in the formulation

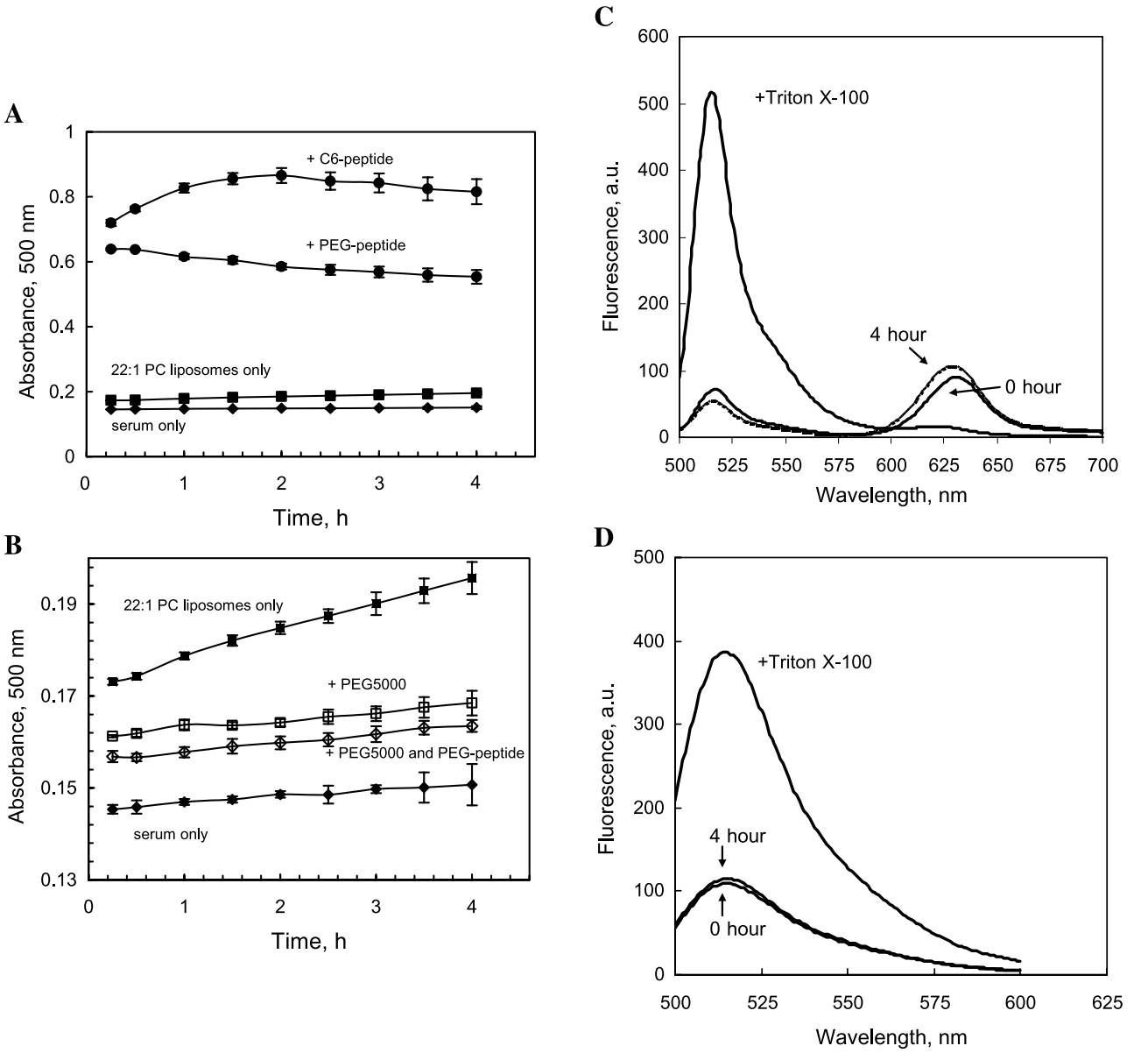

Fig. 1. Biophysical measurements of liposome formulations. (A) Turbidity measurements (absorbance at 500 nm over a 4-h period) indicating serum-induced aggregation when the liposomes of di22:1-PC contained 4 mol% liver-targeting peptide attached to di22:1-aminopropane by a 6-carbon chain ("+ C6-peptide") or on the distal end of PEG_{3400} ("+ PEG–peptide"). Other samples were liposomes of di22:1-PC only and serum only (without liposomes). Absorbance values are mean ± SEM, three separately prepared samples. Turbidity was significantly different from liposomes of 22:1-PC alone for both the C6-peptide formulation ($p = 4 \times 10^{-34}$) and the PEG–peptide formulation ($p = 1 \times 10^{-48}$). (B) Turbidity measurements indicating effective prevention of serum-induced aggregation when 10 mol% di22:1-PE–PEG_{5000} was included in the liposome formulation. Note the much smaller absorbance range compared to (A). Formulations were di22:1-PC only (–■–), serum only (without liposomes) (–◆–), di22:1-PC plus 10 mol% di22:1-PE–PEG_{5000} (–□–), and di22:1-PC plus 10 mol% di22:1-PE–PEG_{5000} plus 4 mol% di-22:1-AP–PEG_{3400}–peptide (–◇–). Absorbance values are mean ± SEM, three separately prepared samples. Both the PEG and the PEG + PEG–peptide formulations exhibited significantly less turbidity compared to liposomes of di22:1-PC alone ($p = 5 \times 10^{-11}$ and $p = 4 \times 10^{-17}$, respectively). (C) Fluorescence measurements indicating low amounts of monomer transfer of fluorescent lipid from liposomes to serum. Liposomes containing 1 mol% each Bodipy-FL and Bodipy-TR-X were incubated in 95% serum at 37°C. Fluorescence spectra (λ_{ex} = 480 nm, λ_{em} = 500 to 700 nm) were recorded at $t = 0$ and $t = 4$ h, then after addition of TX-100 to produce a 2% TX-100 solution. Each scan is the average of three separately prepared samples. (D) Fluorescence measurements indicating insignificant leakage of entrapped calcein dye. Liposomes containing 50 mM calcein were incubated in 95% serum at 37°C. Fluorescence spectra (λ_{ex} = 480 nm, λ_{em} = 500 to 600 nm) were recorded at $t = 0$ and $t = 4$ h, then after addition of TX-100 to produce a 2% TX-100 solution. Each scan is the average of four separately prepared samples.

additional polyethylene glycol chains in the form of di22:1-PE–PEG_{5000}. A liposome formulation of di22:1-PC/di22:1-PE–PEG_{5000}/di22:1-AP–PEG_{3400}–peptide (86:10:4 mol/mol/mol) showed little evidence of turbidity when incubated with serum at 37°C (Fig. 1B), similar to the behavior of the liposomes without peptide, consisting of di22:1-PC/di22:1-PE–PEG_{5000} (90:10) (Fig. 1B).

Stability of the Fluorescent Lipids Within the Liposomes

It was also important to demonstrate that the fluorescent lipids prepared for this investigation remained anchored within the liposomes in the presence of serum, so that they could be used as markers of liposome uptake by various organs. Bodipy-FL and Bodipy-TR-X form an effective fluorescence resonance energy transfer pair, such that significant quenching of Bodipy-FL fluorescence occurs when both fluorophores are present in a liposome bilayer. Fig. 1C shows the fluorescence emission spectrum of liposomes of di22:1-PC/di22:1-PE–PEG_{5000}/di22:1-AP–PEG_{3400}–peptide/di22:1-AP–Bodipy-FL/di22:1-AP–Bodipy-TR-X (84:10:4:1:1) with excitation at 485 nm. The spectrum shows a high degree of quenching of the Bodipy-FL spectrum (λ_{em} = 515 nm) with significant resonance energy transfer to Bodipy-TR-X (λ_{em} = 630 nm). For comparison, the emission spectrum is shown after the addition of Triton X-100, which fully disrupts the liposomes and eliminates energy transfer. When the liposomes were incubated with 95% serum at 37°C, we did observe a statistically significant change in the fluorescence spectrum (Fig. 1C) between 0 and 4 h ($p = 0.0001$). However, this change at the emission maximum of 515 nm was only 4.1 ± 0.1% (mean ± SEM, $n = 3$) of that seen when the liposomes were fully disrupted by Triton X-100, indicating that nearly all of the fluorescent lipid remained within the liposome and did not undergo appreciable monomer lipid transfer into serum components.

Nonleakage of Liposome Contents

The liposome formulations were also evaluated for leakage of entrapped contents to demonstrate their utility as potential drug carriers. Liposomes with the formulation used for liver targeting [di22:1-PC/di22:1-PE–PEG_{5000}/di22:1-AP–PEG_{3400}–peptide (86:10:4)] were prepared in a solution of the fluorescent dye calcein, and the nonentrapped calcein removed by gel filtration. At a concentration of 50 mM, the liposome-entrapped calcein fluorescence is effectively self-quenched. A subsequent increase in fluorescence is taken as a measure of leakage of entrapped dye, as it is diluted in the extraliposomal aqueous compartment (31). Compared to the fluorescence increase seen when the liposomes were fully disrupted with Triton X-100, Fig. 1D shows that the fluorescence spectrum of the calcein-entrapped liposomes changed by only 2.0 ± 0.4% (mean ± SEM, $n = 4$, $p = 0.02$) during a 4-h incubation with 95% serum at 37°C, indicating insignificant contents leakage.

Blood Clearance of Peptide-Containing Liposomes Compared to Control Liposomes

Solutions for *in vivo* administration were prepared containing a mixture of the two liposome formulations described in Table I. These were 1) control liposomes (without peptide) with Bodipy-FL (green fluorescence emission), and 2) peptide-containing liposomes with Bodipy-TR-X (red fluorescence emission). Mice were given i.v. injections of this mixture (0.8 μmol each formulation in a total volume of 80 μL of 5% glucose), and blood samples taken at various times between 15 min and 1.5 h for analysis of the fluorescence content of the serum. As seen in Fig. 2A, relative to control liposomes, peptide-containing liposomes were largely cleared from blood within the first 15 min after injection. Analysis of variance indicated that no further blood clearance occurred between the 15 and 90-min time points ($p = 0.48$), whereas the clearance during the first 15 min was highly statistically significant ($p = 1.6 \times 10^{-19}$).

Organ Uptake of Peptide-Containing Liposomes

At 15 min postinjection, animals were deeply anesthetized and perfused intravascularly with saline. Liver, lungs, spleen, kidneys, and heart were collected and carried through a lipid-extraction procedure (described in "Materials and Methods") to measure quantitatively uptake of both peptide-containing liposomes and control liposomes.

Representative fluorescence emission scans of Bodipy-TR-X (from the peptide-containing liposomes) of the tissue lipid extracts obtained from these experiments are shown in Fig. 2B. Substantial uptake of the peptide-containing liposomes, per gram of tissue, was measured in liver and spleen, with negligible uptake by lungs, kidneys, and heart.

Figure 2C presents the results of the quantitative analysis of the liposome uptake expressed as a percentage of the total injected dose. Uptake of control liposomes was low in all organs. Uptake of peptide-containing liposomes occurred primarily in liver, averaging 77% of the total injected dose. Quantitatively, the uptake of peptide-containing liposomes by the liver was 676-fold higher compared to heart ($p = 0.00006$, paired, two-tailed t test), 194-fold higher compared to kidney ($p = 0.00006$), 277-fold higher compared to lung ($p = 0.00006$), and 12-fold higher compared to spleen ($p = 0.0001$).

In Fig. 2D the data are expressed per gram of tissue. By this measure, the uptake of peptide-containing liposomes by the liver was 79-fold higher compared to heart ($p = 0.0004$), 457-fold higher compared to a sample of adipose tissue ($p = 0.0004$), 58-fold higher compared to kidney ($p = 0.0003$), 52-fold higher compared to lung ($p = 0.0004$), but only 1.3-fold higher compared to spleen ($p = 0.06$, not statistically significant).

Light and Electron Microscopy

In addition to the blood clearance and tissue extractions described above, tissue samples (18 mice total) were also fixed with formaldehyde and examined by fluorescence microscopy. At 1.5 h after i.v. injection, the Bodipy-TR-X in the peptide-containing liposomes produced prominent red fluorescence along the sinusoidal borders throughout the liver (Fig. 3A). Substantial fluorescence was also seen within the cytoplasm of hepatocytes, compared to its total absence within the nuclei (Fig. 3A). Liver and hepatocyte labeling by the Bodipy-FL (green emission) in the control liposomes was

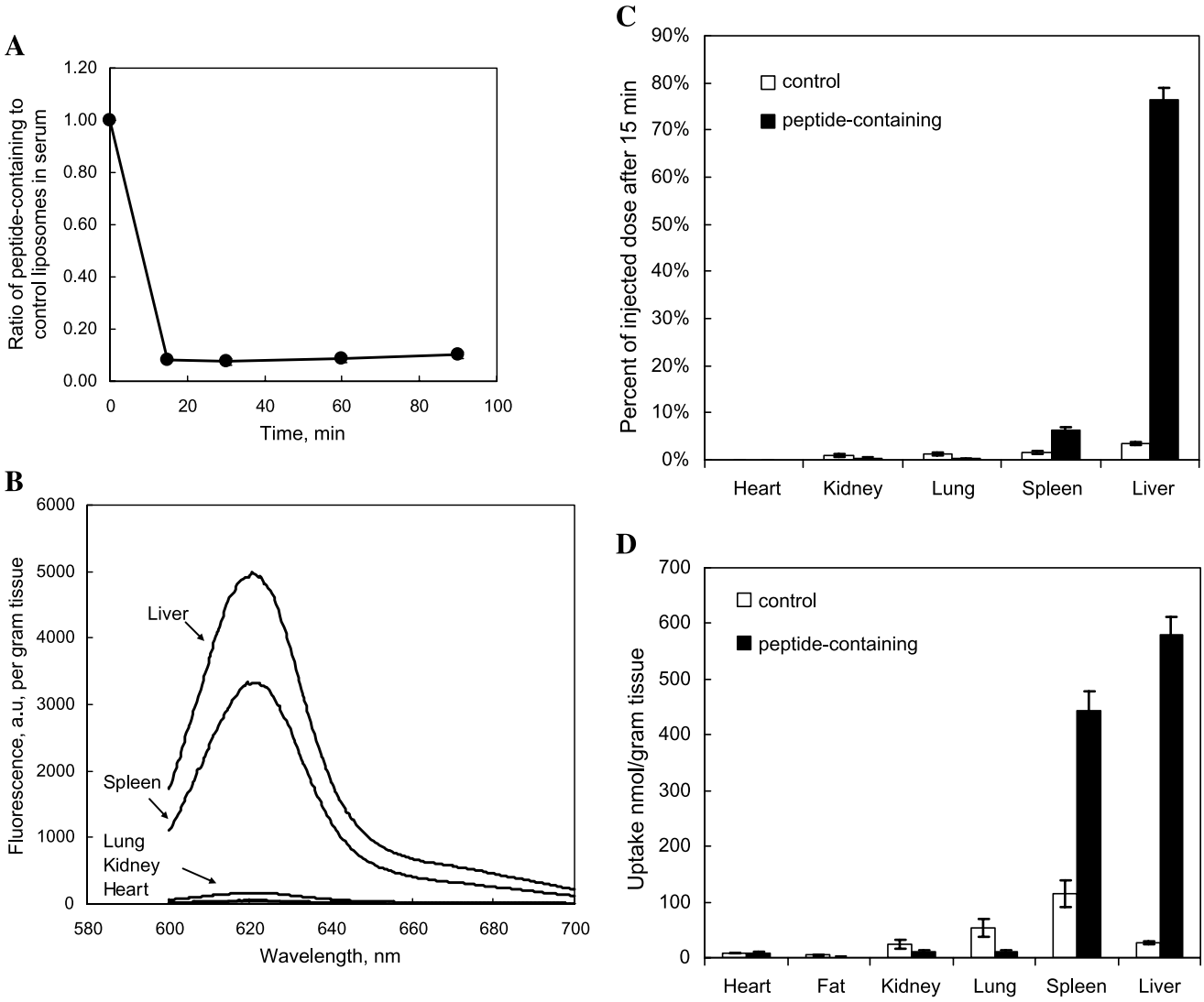

Fig. 2. Rapid clearance of peptide-containing liposomes from blood and preferential uptake by liver. Each BALB/c mouse was injected via the tail vein with a solution containing equal quantities (0.8 μmol each) of 1) liposomes containing liver-targeting peptide plus Bodipy-TR-X fluorescent label, and 2) control liposomes without peptide but with Bodipy-FL fluorescent label. See Table I for liposome compositions. (A) Clearance of peptide-containing liposomes from blood relative to control liposomes. Time = 0, ratio of peptide-containing liposomes to control liposomes prior to injection, determined by fluorescence intensities, normalized to 1. Later times, ratio of peptide-containing liposomes to control liposomes in serum at indicated times, normalized by the fluorescence intensities prior to injection. Data are mean ± SEM, $n = 4$ mice. In most cases, error bars are smaller than symbol size. (B) Representative Bodipy-TR-X fluorescence scans of lipid extracts of various organs showing uptake of peptide-containing liposomes after 15 min. Uptake was highest in liver, less in spleen, and negligible in kidney, lung, and heart. (C) Quantitative uptake (after 15 min) of peptide-containing liposomes (solid bars) by various organs compared to control liposomes (open bars) expressed as a percentage of total injected dose. Values are mean ± SEM, $n = 4$ mice. (D) Quantitative uptake (after 15 min) of peptide-containing liposomes (solid bars) by various organs compared to control liposomes (open bars) expressed as nmol liposomes per gram tissue. Values are mean ± SEM, $n = 4$ mice.

virtually absent (Fig. 3B). Patterns of labeling similar to that illustrated in Fig. 3 were seen in liver sections from animals euthanized shortly after i.v. injection (15 min) and as long as 4 h after injection (data not shown). Fluorescence microscopy of other tissues revealed modest levels of red fluorescence (from peptide-containing liposomes) in spleen and no detectable red fluorescence in lung, kidney, and heart (data not shown).

Note that in all of the above experiments (Fig. 2A–D and Fig. 3A and B), peptide-containing liposomes (with Bodipy-TR-X) and control liposomes (with Bodipy-FL) were mixed and injected simultaneously into each animal. In separate experiments (data not shown), control liposomes and peptide-containing liposomes were administered alone, rather than in combination. For animals treated with peptide-containing liposomes (containing Bodipy-TR-X), light microscopic images of liver tissue were identical to those seen in Fig. 3A, showing strong labeling of liver tissue. For animals treated with control liposomes only (containing Bodipy-FL), light microscopic images of liver tissue were identical to those seen in Fig. 3B, showing virtually no uptake of control liposomes.

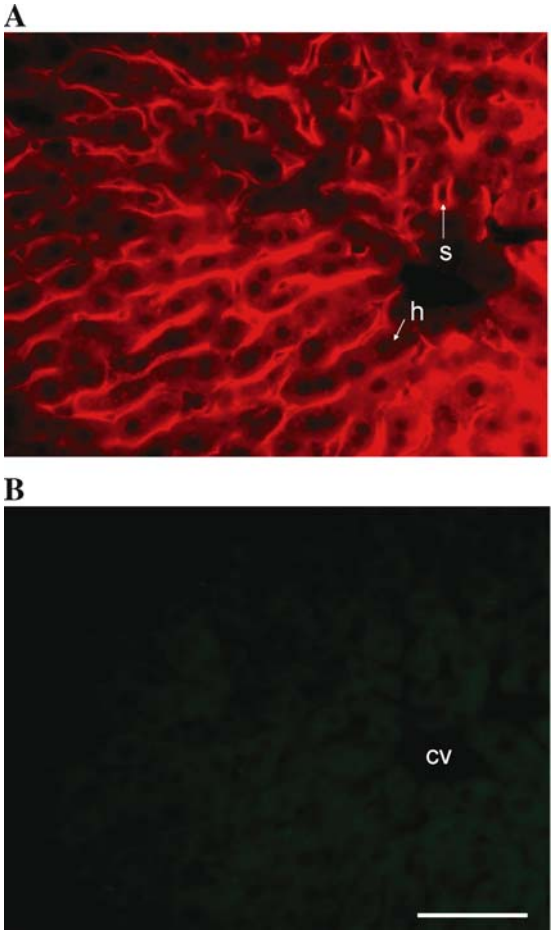

Fig. 3. Fluorescence photomicrographs of 12 μm thick cryostat sections from liver of a BALB/c mouse. The animal was injected via the tail vein with equal quantities (0.8 μmol total lipid) of 1) liposomes containing liver-targeting peptide plus Bodipy-TR-X fluorescent label (red emission) and 2) control liposomes without liver-targeting peptide but with Bodipy-FL fluorescent label (green emission). The animal was euthanized 90 min after injection, followed by saline perfusion, followed by formaldehyde perfusion. (A) Section of liver seen under rhodamine optics suitable for illumination of Bodipy-TR-X from peptide-containing liposomes. Photomicrograph shows substantial fluorescence throughout hepatocyte cells (with exception of nuclei) plus prominently labeled regions adjacent to sinusoidal capillaries. (B) Same section as in (A), with equal exposure time, seen under fluorescein optics suitable for illumination of Bodipy-FL from control liposomes. Note absence of labeling. cv, central vein; h, hepatocyte; s, sinusoidal capillary. Calibration bar in (B) = 50 μm.

In a separate experiment, mice were injected i.v. with peptide-containing liposomes with 0.1% gold-particle-labeled phosphatidylethanolamine. Liver tissue was harvested after 15 min, 1.5 h, and 4 h, then processed for gold enhancement and electron microscopy. Gold particles were observed associated with the plasma membrane and within the cytoplasm of endothelial and Kupffer cells forming the sinusoidal lining (Fig. 4A). Gold particles were also observed associated with hepatocytes (Fig. 4A and B), including the plasma membrane bordering the space of Disse, the cytoplasm, and especially associated with cytoplasmic membranes. In contrast, gold particles were never seen within cell nuclei of any cell type. This is indicated in Fig. 4B, which shows a portion of a Kupffer cell, with gold particle labeling within the cytoplasm but not the nucleus. Counting of gold particles per unit area of cytoplasm indicated 23.0 ± 2.0 (mean ± SEM) gold particles per 0.25 μm^2 of hepatocyte. In contrast, 45.2 ± 3.3 (mean ± SEM) particles per 0.25 μm^2 were observed within the cells lining the sinusoids (endothelial + Kupffer cells). This 2-fold difference between parenchymal and nonparenchymal cells was statistically significant (p = 0.0001).

Liposome Binding to Enzyme-Treated Liver Slices

To investigate the interaction of the liposomes with extracellular matrix molecules found in liver tissue, liver slices were treated with chondroitinase ABC or heparinase.

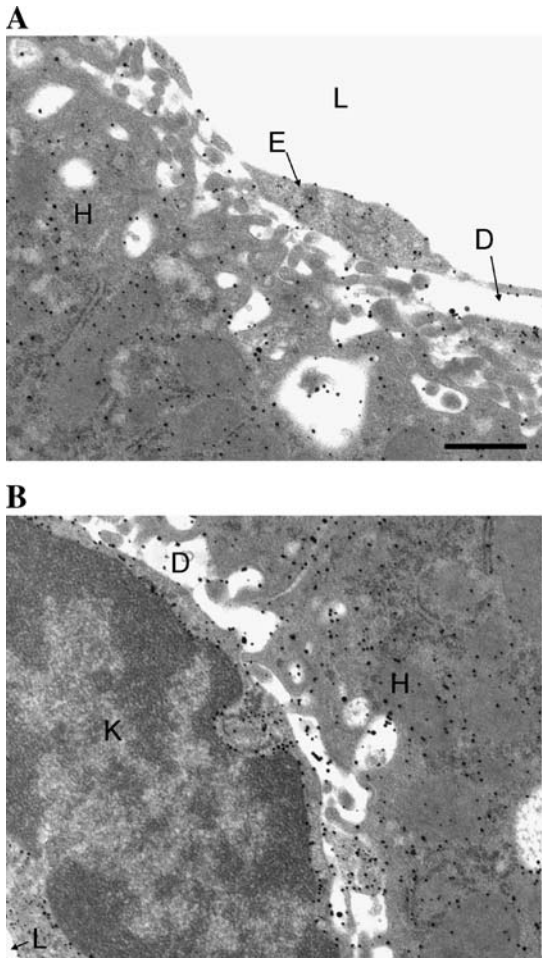

Fig. 4. Electron micrographs of liver sections of BALB/c mouse processed for enhancement of gold label of liposomes. The animal was injected via the tail vein with liposomes (0.8 μmol total lipid) containing liver-targeting peptide plus 0.1% gold-labeled phosphatidylethanolamine, and euthanized after 1.5 h. (A) Border of sinusoidal capillary. Note gold particles overlying cytoplasm of an endothelial cell (E) and cytoplasm of a hepatocyte (H). L, lumen of sinusoidal capillaries; D, space of Disse. (B) Gold particles overlying cytoplasm of a Kupffer cell (K); note absence of label over the nucleus. Gold particles also seen over the space of Disse (D) and over the cytoplasm of hepatocytes (H). Calibration bar in (A) = 0.5 μm.

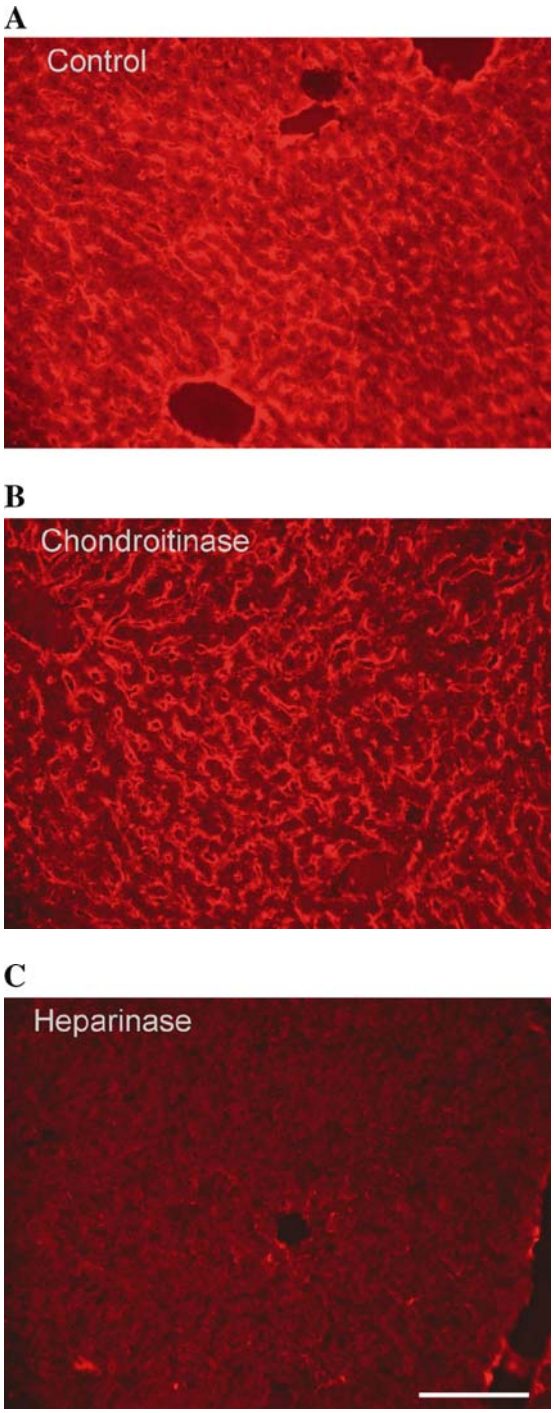

Fig. 5. Fluorescence photomicrographs of 12-μm-thick cryostat sections from liver of a BALB/c mouse. Sections were obtained following paraformaldehyde fixation as described in "Materials and Methods." After control or enzyme treatment, liver slices were incubated for 1 h at 37 °C with peptide-containing liposomes, washed, and viewed with rhodamine optics suitable for illumination of Bodipy-TR-X. (A) Control liver slice not subjected to enzyme treatment, showing labeling of sinusoidal and hepatocyte basolateral regions. (B) Photomicrograph of liver slice, with equal exposure time as (A), treated 2 h with chondroitinase ABC prior to liposome binding. (C) Photomicrograph of liver slice, with equal exposure time as (A), treated 2 h with heparinase prior to liposome binding. Calibration bar in (C) = 100 μm.

The photomicrograph in Fig. 5A shows a control liver slice (without enzyme treatment) after a 1-h incubation with peptide-containing liposomes. The image shows a pattern of fluorescence that is remarkably similar to the pattern seen in sections taken from animals in which peptide-containing liposomes were injected intravenously. In particular, liposome fluorescence appears along the sinusoidal borders and along the basolateral region of the hepatocytes adjacent to the sinusoids. Liver slices treated with control liposomes (without peptide) showed essentially no liposome binding (data not shown).

Figure 5B shows a liver slice treated with 10 U/mL chondroitinase ABC for 2 h prior to a 1-h incubation with peptide-containing liposomes. Similar to the control experiment, the pattern of fluorescence in Fig. 5B also shows clear fluorescence labeling along the sinusoidal borders. In contrast, Fig. 5C presents an example of a liver slice treated with 2.5 U/mL heparinase for 2 h prior to incubation with peptide-containing liposomes. The enzyme treatment virtually eliminated liposome binding. These experiments suggest that the liposome binding to liver tissue was specific to the HSPGs found in the sinusoidal and hepatocyte basolateral regions. These experiments also indicate that opsonization is not a likely mechanism of uptake of liposomes by liver. The liver slice experiments were performed in serum-free buffer, hence adsorption of serum protein by liposomes is not required for the binding of the liposomes to liver tissue.

DISCUSSION

The CSP present on the surface of *Plasmodium* sporozoites contains two conserved amino sequences named region I and region II. Region I consists of an invariant five-amino-acid sequence, KLKQP, and is found in *Plasmodium* species that target the liver during the initial phase of host invasion (32). The CSPs from various species also contain, upstream from region I, at least one HSPG consensus binding sequence. Peptides containing both the HSPG binding sequence and amino acids KLKQP have been named "region I-plus" (9).

Here we show that a 19-amino acid sequence from the region I-plus of the CSP of *P. berghei*, when presented as an array of peptide extending from the surface of a lipid bilayer, is sufficient to direct a remarkably selective and efficient targeting of systemically administered liposomes to mouse liver *in vivo*. The uptake of liposomes by liver was several hundredfold higher compared to the heart, kidneys, and lungs, and more than 10-fold higher compared to spleen. However, when the data were expressed per gram of tissue, we did note a similar uptake by both liver and spleen. Spleen contains macrophages that are part of the reticular endothelial system that, as one of its functions, carries out particle clearance from the circulation. This may account for at least part of the accumulation of liposomes seen in that organ.

The most significant difficulty we encountered during the development of an effective liposome formulation for *in vivo* administration was the tendency of this targeting peptide to induce rapid aggregation when the liposomes were mixed with serum. This aggregation occurred even if the peptide was incorporated onto the distal end of PEG_{3400}. We found that surrounding the targeting peptide with additional chains

of PEG_{5000} without peptide, in a 2.5:1 ratio, effectively eliminated aggregation. In addition, the use of the long-chain C22:1 fatty acid in all components resulted in liposomes that were nonleaky in the presence of serum, even when the liposomes contained relatively high mole fractions of PEG (10% PEG_{5000} plus 4% PEG_{3400}–peptide). We are not aware of other systems where liposomes containing targeting ligands have been stabilized by the inclusion of additional polyethylene glycol chains without ligand. However, given the successful outcome we achieved, we suggest that other investigators who are developing nanoparticle systems for therapeutic use consider incorporating combinations of PEG chains with and without targeting ligands, with the goal of stabilizing formulations that are otherwise unstable in the presence of serum and blood. In our studies, this stability allowed for the passage of considerable quantities of liposome material beyond the sinusoidal lining of the liver and into the hepatocytes. Based upon quantitative analysis of gold particles visualized by electron microscopy, we found the amount of liposome material in the cells of the sinusoidal lining (endothelial + Kupffer cells) was approximately 2-fold higher per unit area compared to the parenchymal cells (hepatocytes). Because the total volume occupied by hepatocytes has been reported to be approximately 12 times the volume occupied by endothelial and Kupffer cells (28), our results suggest that more than 80% of the liposome material delivered to the liver was contained within the hepatocytes.

To date, most targeted liposomal systems developed for delivery specifically to liver have incorporated ligands intended to recognize the asialoglycoprotein receptor (ASGP-R) on the basolateral side of hepatocytes. These strategies have been recently reviewed (33) and include formulations that contain glycosylated proteins such as asialofetuin, clusters of galactose or lactose linked to various lipophilic anchors, and various synthetic, carbohydrate-containing polymers. The ability of liposome formulations to target the ASGP-R seems to be highly dependent not only on the particular composition and geometry of the targeting motif (34), but upon the overall composition as well (35–37). For example, liposomes containing the galactosylated cholesterol derivative Gal-C4-Chol are rapidly eliminated from blood and accumulate in liver when present in liposomes of distearoylphosphatidylcholine and cholesterol (60:40), but not when long-chain polyethylene glycol is included in the formulation (38). Many liposome preparations without targeting ligand (without polyethylene glycol) also accumulate in liver through a variety of pathways such as opsonization and nonspecific electrostatic interactions (35,39), which complicates the evaluation of the role of ASGP-R in liposome accumulation relative to other mechanisms. As a result, it is difficult to make clear distinctions between liposome targeting strategies based upon recognition of ASGP-R and the results we report here. At this time, we conclude that the most significant difference seems to be that the liver-targeting peptide we have developed for this investigation is remarkably effective in a liposome preparation that is well stabilized with polyethylene glycol chains.

To develop this peptide-based targeted delivery system for eventual therapeutic use, particularly for repeat administration, the potential antigenicity of the system must be investigated. Our immediate research plans are to develop ELISA tests to detect antibodies present in the host following repeat administration. In addition, our research objective is to determine the minimum amino acid sequence required for targeting. This objective should lead to the development of delivery systems more suitable for the host, as shorter peptides are, in general, less antigenic. Shorter peptides are also needed for a more careful evaluation of the mechanism of targeting, as nonessential amino acids present in our current 19-amino-acid peptide will be eliminated, and variants of the essential sequence, such as scrambled sequences, can be more intelligently designed and studied.

Plasmodium is only one of a variety of microorganisms that have been shown to seek out specific target organs and tissues *in vivo* by recognition of specific extracellular and cell-surface glycosaminoglycans (15). In addition, selective recognition of glycosaminoglycans is used by endogenous ligands to carry out numerous physiological functions (13). The relative amounts and the fine structures of the glycosaminoglycans vary considerably among the different organs and cell types in which they are found (40–43). Selective recognition of these molecules with appropriately designed ligands offers the possibility of selective targeting of therapeutic nanoparticles to a variety of organs and cell types in the mammalian host. To date, only limited work has been carried out in this area. Given the success of this strategy both in normal physiology and in host invasion by microorganisms, it seems that this is an area of drug delivery research that could prove very rewarding for the development of targeted delivery systems.

ACKNOWLEDGMENTS

This work was supported by the National Institutes of Health EB-003075. The authors thank Dr. E. Wisse for his very informative personal communications regarding liver anatomy and fine structure.

REFERENCES

1. E. Wisse. An electron microscopic study of the fenestrated endothelial lining of rat liver sinusoids. *J. Ultrastruct. Res.* **31**:125–150 (1970).
2. E. Wisse, R. B. DeZanger, K. Charels, P. van der Smissen, and R. S. McCuskey. The liver sieve: considerations concerning the structure and function of endothelial fenestrae, the sinusoidal wall and the space of Disse. *Hepatology* **5**:683–692 (1985).
3. U. Frevert. Malaria sporozoite–hepatocyte interactions. *Exp. Parasitol.* **79**:206–210 (1994).
4. R. Ménard. The journey of the malaria sporozoite through its hosts: two parasite proteins lead the way. *Microbes Infect.* **2**:633–642 (2000).
5. M. M. Mota and A. Rodriguez. Invasion of mammalian host cells by *Plasmodium* sporozoites. *Bioessays* **24**:149–156 (2002).
6. S. C. Shin, J. P. Vanderberg, and J. A. Terzakis. Direct infection of hepatocytes by sporozoites of *Plasmodium berghei*. *J. Protozool.* **29**:448–454 (1982).
7. E. Ungureanu, R. Killick-Kendrick, P. C. Garnham, P. Branzei, C. Romanescu, and P. G. Shute. Prepatent periods of a tropical strain of *Plasmodium vivax* after inoculations of tenfold dilutions of sporozoites. *Trans. R. Soc. Trop. Med. Hyg.* **70**: 482–483 (1977).
8. R. Tewari, R. Spaccapelo, F. Bistoni, A. A. Holder, and A. Crisanti. Function of region I and II adhesive motifs of

Plasmodium falciparum circumsporozoite protein in sporozoite motility and infectivity. *J. Biol. Chem.* **277**:47613–47618 (2002).
9. J. B. Ancsin and R. Kisilevsky. A binding site for highly sulfated heparan sulfate is identified in the N terminus of the circumsporozoite protein: significance for malarial sporozoite attachment to hepatocytes. *J. Biol. Chem.* **279**:21824–21832 (2004).
10. M. Lyon, J. A. Deakin, and J. T. Gallagher. Liver heparan sulfate structure. A novel molecular design. *J. Biol. Chem.* **269**:11208–11215 (1994).
11. U. Frevert, P. Sinnis, P. C. Cerami, W. Shreffler, B. Takacs, and V. Nussenzweig. Malaria circumsporozoite protein binds to heparan sulfate proteoglycans associated with the surface membrane of hepatocytes. *J. Exp. Med.* **177**:1287–1298 (1993).
12. G. Pradel, S. Garapaty, and U. Frevert. Proteoglycans mediate malaria sporozoite targeting to the liver. *Mol. Microbiol.* **45**: 637–651 (2002).
13. M. Bernfield, M. Gotte, P. W. Park, O. Reizes, M. L. Fitzgerald, J. Lincecum, and M. Zako. Functions of cell surface heparan sulfate proteoglycans. *Annu. Rev. Biochem.* **68**:729–777 (1999).
14. J. D. Esko and S. B. Selleck. Order out of chaos: assembly of ligand binding sites in heparan sulfate. *Annu. Rev. Biochem.* **71**:435–471 (2002).
15. K. S. Rostand and J. D. Esko. Microbial adherence to and invasion through proteoglycans. *Infect. Immun.* **65**:1–8 (1997).
16. M. Belting. Heparan sulfate proteoglycan as a plasma membrane carrier. *Trends Biochem. Sci.* **28**:145–151 (2003).
17. I. Sauer, I. R. Dunay, K. Weisgraber, M. Bienert, and M. Dathe. An apolipoprotein E-derived peptide mediates uptake of sterically stabilized liposomes into brain capillary endothelial cells. *Biochemistry* **44**:2021–2029 (2005).
18. Z. M. Ding, R. Cristiano, J. A. Roth, B. Takacs, and M. T. Kuo. Malarial circumsporozoite protein is a novel gene delivery vehicle to primary hepatocyte cultures and cultured cells. *J. Biol. Chem.* **270**:3667–3676 (1995).
19. C. G. Fields, D. H. Lloyd, R. I. Macdonald, K. M. Otteson, and R. L. Noble. HBTU activation for automated Fmoc solid-phase peptide synthesis. *Pept. Res.* **4**:95–101 (1991).
20. E. A. Murphy, A. J. Waring, S. M. Haynes, and K. J. Longmuir. Compaction of DNA in an anionic micelle environment followed by assembly into phosphatidylcholine liposomes. *Nucleic Acids Res.* **28**:2986–2992 (2000).
21. C. A. Guy and G. B. Fields. Trifluoroacetic acid cleavage and deprotection of resin-bound peptides following synthesis by Fmoc chemistry. *Methods Enzymol.* **289**:67–83 (1997).
22. R. C. Beavis, T. Chaudhary, and B. T. Chait. Alpha-cyano-4-hydroxycinnamic acid as a matrix for matrix-assisted laser desorption mass-spectrometry. *Org. Mass Spectrom.* **27**:156–158 (1992).
23. R. Sato, Y. Itabashi, H. Fujishima, H. Okuyama, and A. Kuksis. Simple synthesis of diastereomerically pure phosphatidylglycerols by phospholipase D-catalyzed transphosphatidylation. *Lipids* **39**:1025–1030 (2004).
24. J. Otera. *Esterification: Methods, Reactions, and Applications*, Wiley-VCH, Weinheim, 2003.
25. E. Wisse. An electron microscopic study of the fenestrated endothelial lining of rat liver sinusoids. *J. Ultrastruct. Res.* **31**:125–150 (1970).
26. E. Wisse. An ultrastructural characterization of the endothelial cell in the rat liver sinusoid under normal and various experimental conditions, as a contribution to the distinction between endothelial and Kupffer cells. *J. Ultrastruct. Res.* **38**:528–562 (1972).
27. E. Wisse. Observations on the fine structure and peroxidase cytochemistry of normal rat liver Kupffer cells. *J. Ultrastruct. Res.* **46**:393–426 (1974).
28. A. Blouin, R. P. Bolender, and E. R. Weibel. Distribution of organelles and membranes between hepatocytes and nonhepatocytes in the rat liver parenchyma. A stereological study. *J. Cell Biol.* **72**:441–455 (1977).
29. E. G. Bligh and W. J. Dyer. A rapid method of total lipid extraction and purification. *Can. J. Biochem. Physiol.* **37**:911–917 (1959).
30. J. R. Lakowicz. *Principles of Fluorescence Spectroscopy*, 2nd ed., Kluwer Academic/Plenum Publishers, New York, 1999.
31. D. H. Haas and R. M. Murphy. Design of a pH-sensitive pore-forming peptide with improved performance. *J. Pept. Res.* **63**:9–16 (2004).
32. T. F. McCutchan, J. C. Kissinger, M. G. Touray, M. J. Rogers, J. Li, M. Sullivan, E. M. Braga, A. U. Krettli, and L. H. Miller. Comparison of circumsporozoite proteins from avian and mammalian malarias: biological and phylogenetic implications. *Proc. Natl. Acad. Sci. USA* **93**:11889–11894 (1996).
33. J. Wu, M. H. Nantz, and M. A. Zern. Targeting hepatocytes for drug and gene delivery: emerging novel approaches and applications. *Front. Biosci.* **7**:d717–d725 (2002).
34. M. Nishikawa. Development of cell-specific targeting systems for drugs and genes. *Biol. Pharm. Bull.* **28**:195–200 (2005).
35. G. L. Scherphof, G. Koning, M. Bartsch, X. Yan, and J. Kamps. Targeting liposomes and lipoplexes to cells in the liver. *Cell. Mol. Biol. Lett.* **7**:251–254 (2002).
36. A. Murao, M. Nishikawa, C. Managit, J. Wong, S. Kawakami, F. Yamashita, and M. Hashida. Targeting efficiency of galactosylated liposomes to hepatocytes *in vivo*: effect of lipid composition. *Pharm. Res.* **19**:1808–1814 (2002).
37. T. Daemen, M. Velinova, J. Regts, M. deJager, R. Kalicharan, J. Donga, J. J. van der Want, and G. L. Scherphof. Different intrahepatic distribution of phosophatidylglycerol and phosphatidylserine liposomes in the rat. *Hepatology* **26**:416–423 (1997).
38. C. Managit, S. Kawakami, M. Nishikawa, F. Yamashita, and M. Hashida. Targeted and sustained drug delivery using PEGylated galactosylated liposomes. *Int. J. Pharm.* **266**:77–84 (2003).
39. J. A. A. M. Kamps and G. L. Scherphof. Biodistribution and uptake of liposomes *in vivo*. *Methods Enzymol.* **387**:257–266 (2004).
40. M. Kato, H. Wang, M. Bernfield, J. T. Gallagher, and J. E. Turnbull. Cell surface syndecan-1 on distinct cell types differs in fine structure and ligand binding of its heparan sulfate chains. *J. Biol. Chem.* **269**:18881–18890 (1994).
41. U. Lindahl, M. Kusche-Gullberg, and L. Kjellen. Regulated diversity of heparan sulfate. *J. Biol. Chem.* **273**:24979–24982 (1998).
42. M. P. Hoffman, J. A. Engbring, P. K. Nielsen, J. Vargas, Z. Steinberg, A. J. Karmand, M. Nomizu, Y. Yamada, and H. K. Kleinman. Cell type-specific differences in glycosaminoglycans modulate the biological activity of a heparin-binding peptide (RKRLQVQLSIRT) from the G domain of the laminin alpha1 chain. *J. Biol. Chem.* **276**:22077–22085 (2001).
43. S. Knox, C. Merry, S. Stringer, J. Melrose, and J. Whitelock. Not all perlecans are created equal: interactions with fibroblast growth factor (FGF) 2 and FGF receptors. *J. Biol. Chem.* **277**:14657–14665 (2002).